

Tuning Paramagnetic Spin Excitations of Single Adatoms

Julen Ibañez-Azpiroz,* Manuel dos Santos Dias, Benedikt Schweflinghaus, Stefan Blügel, and Samir Lounis[†]

Peter Grünberg Institute and Institute for Advanced Simulation, Forschungszentrum Jülich & JARA, D-52425 Jülich, Germany

(Received 13 February 2017; published 7 July 2017)

We predict the existence of paramagnetic spin excitations (PSE) in nonmagnetic single adatoms. Our calculations demonstrate that PSE develop a well-defined structure in the meV region when the adatom's Stoner criterion for magnetism is close to the critical point. We further reveal a subtle tunability and enhancement of PSE by external magnetic fields. Finally, we show how PSE can be detected as moving steps in the dI/dV signal of inelastic scanning tunneling spectroscopy, opening a potential route for experimentally accessing electronic properties of nonmagnetic adatoms, such as the Stoner parameter.

DOI: 10.1103/PhysRevLett.119.017203

Single adatoms deposited on surfaces have become a prominent playground where theory and experiment can explore hand by hand a large variety of physical phenomena ranging from spin excitations [1–10] to magnetic exchange interactions [11–13], quantum spin decoherence [14–16], topological superconductivity [17–19], or the Kondo effect [20,21], among many others. Virtually all of these effects arise from the intricate interplay between the degrees of freedom of the adatom—charge, spin, or orbital momentum—and the electron and phonon bath of the substrate, a subject of heavy and ongoing investigation.

Noteworthily, magnetism plays a central role in fueling the interest for single adatoms, given that they represent the ultimate limit in the context of bit miniaturization in data storage devices. As a consequence, great efforts are being devoted to the search and characterization of elements that become magnetic when deposited on a substrate. Successful examples include, e.g., Fe and Co on Pt(111) [7,22], Fe on Cu(111) [6] as well as on Cu₂Ni/Cu(111) [23] and CuNi [1], Co on MgO(100) [24], and more recently Ho on MgO/Ag(100) [25], which all exhibit local magnetic moments greater than $2\mu_B$ and reveal clear signatures of magnetism that manifest either in a large magnetic anisotropy energy, steps in the dI/dV signal related to spin excitations, or even remanence of the magnetic signal.

In this Letter, we propose and argue that even nominally nonmagnetic single adatoms can exhibit clear fingerprints of magnetism in the form of well-defined features in the spin-excitation spectrum, i.e., paramagnetic spin excitations (PSE). Interestingly, PSE are the analogous of so-called paramagnons first proposed by Doniach in 1967 [26] and first measured in bulk Pd nearly 50 years later by Doubble *et. al.* [27] (see also Ref. [28] for recent calculations). In the context of Fermi liquid theory, these excitations can be viewed as persistent spin-fluctuation modes that can be activated by temperature and thus produce a measurable impact on properties such as specific heat or electron effective-mass enhancement [26,29]. Upon reducing the dimensionality of the system, here we show that PSE can be

strongly enhanced due to the modified interplay between the two fundamental electronic properties involved, namely the Stoner exchange interaction and the adatom's density of states (DOS) at the Fermi level. Importantly, this opens up unforeseen potential applications of nonmagnetic adatoms in nanotechnology, which encodes and manipulates information into excitation modes like PSE. In addition, our ab initio analysis based on time-dependent density functional theory (TDDFT) reveals that PSE are highly sensitive to externally applied magnetic fields and, furthermore, can exhibit a singular enhancement when the field approaches a critical regime. Motivated by these findings, we assess the impact of PSE on the dI/dV signal as measured in inelastic scanning tunneling spectroscopy (ISTS) experiments, identifying clear signatures of magnetic response that allow us to distinguish these types of excitations from, e.g., phonons.

A central property for our discussion is the spin-excitation spectrum of nonmagnetic adatoms. Within the TDDFT formalism, this information is encoded into the longitudinal component of the enhanced spin susceptibility, $\chi(\omega)$, which is related to the response of the noninteracting Kohn-Sham (KS) system, $\chi^{KS}(\omega)$ [30]:

$$\chi(\omega) = \frac{\chi^{KS}(\omega)}{1 - I_{s}\chi^{KS}(\omega)}.$$
 (1)

Above, I_s denotes the so-called Stoner parameter, which plays the role of the exchange-correlation kernel in the adiabatic local spin-density approximation [31]. Noteworthily, the static limit of Eq. (1) recovers the standard Stoner theory that provides the well-known criterion for magnetism, i.e., $\chi(0) < 0 \Rightarrow I_s \rho_F > 1$, with ρ_F the adatom's DOS at the Fermi level and we used $\chi^{KS}(0) = \rho_F > 0$ [30]. In essence, the product $I_s \rho_F$ quantifies the competition between the exchange interaction, which enhances the tendency towards magnetism of electrons in localized orbitals, and substrate hybridization, which induces delocalization of the adatom's electrons and therefore acts against magnetism, thus playing the role of the kinetic

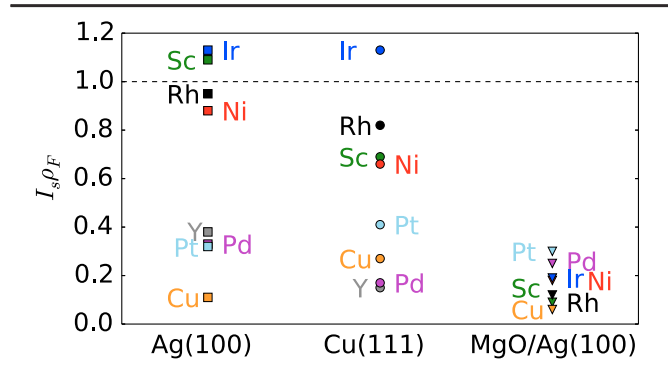


FIG. 1. Calculated Stoner product for various 3d, 4d, and 5d transition metal adatoms deposited on Ag(100) (squares), Cu(111) (circles), and MgO/Ag(100) (triangles).

energy in the standard Stoner theory. It is interesting to note that even if an adatom does not fulfill the Stoner criterion, it can still develop dynamical PSE provided the details of the electronic structure make the denominator of Eq. (1) vanishingly small at a finite frequency.

Let us begin our analysis by characterizing the set of 3d, 4d, and 5d transition metal adatoms that could potentially exhibit PSE. For this purpose, in Fig. 1 we list several adatoms whose calculated Stoner products are below or slightly above 1; the calculations have been performed following the Korringa-Kohn-Rostoker Green function formalism [4,32,33] (see Supplemental Material [34] for technical details) and considering three different substrates, namely Ag(100), Cu(111), and MgO/Ag(100). As a general trend, our calculations show that the metallic substrates Ag(100) and Cu(111) host adatoms whose Stoner product is closer to the critical value 1 as compared to insulating MgO/Ag(100). This is mainly due to the small ρ_F in the later, as tabulated in the Supplemental Material [34]. Among the two metallic substrates, Ag(100) hosts adatoms whose Stoner product are closest to 1, with $I_s \rho_F$ ranging between \sim [1 – 0.1, 1 + 0.1] for Sc, Ir, Rh, and Ni adatoms. Therefore, throughout the work we will focus on discussing the Ag(100) substrate in detail, as it illustrates best our findings.

In Fig. 2 we illustrate the calculated spin-excitation spectra as given by $\text{Im}\chi(\omega)$ from Eq. (1), where all calculations were done considering the nonmagnetic ground state (see Supplemental Material [34] for technical details). Interestingly, Fig. 2 reveals peaklike structures resonating at frequencies below 100 meV for Rh, Ni, Ir, and Sc adatoms. This is exceptional, as most nonmagnetic elements exhibit a featureless spectrum owing to a complete overdamping of the excitations. Rh represents the most favorable case, displaying a well-defined peak at $\omega_{\rm res} \sim 20$ meV and a width of $\Delta \sim 50$ meV, the associated lifetime being $\tau = \omega_{\rm res}^{-1} \sim 30$ fs. It is noteworthy that both the lifetime and the height of the peak, the later being related to the intensity of the excitation, are only one order of magnitude smaller than those of usual transverse spin-excitations

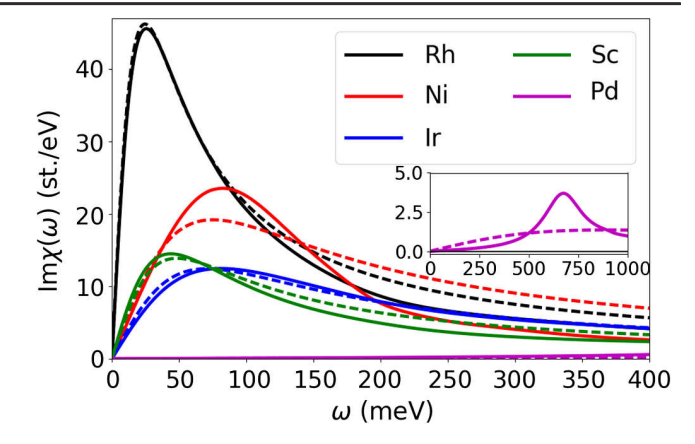


FIG. 2. Solid lines illustrate the calculated density of PSE as given by $\text{Im}\chi(\omega)$ [Eq. (1)] of selected 3d, 4d, and 5d transition metal adatoms deposited on the metallic Ag(100) substrate. Dashed lines denote the approximation of Eq. (2). Note that both Eqs. (1) and (2) give rise to PSE.

measured by ISTS in magnetic adatoms, such as Fe on Cu(111) (see, e.g., Refs. [6,40]). On the other extreme, Pd in Fig. 2 shows a highly overdamped resonance at around 600 meV (see figure inset) whose intensity is an order of magnitude smaller than that of Rh. Therefore, our *ab initio* calculations reveal the existence of PSE whose resonance frequency and width vary strongly depending on the adatom.

Next, we focus on characterizing the physical mechanism behind PSE that allows an interpretation of the *ab initio* results displayed in Fig. 2. For this purpose, let us consider the frequency expansion of the paramagnetic KS spin response function up to linear order, i.e., $\chi^{KS}(\omega) = \rho_F + i\alpha\omega + \mathcal{O}(\omega^2)$. One can show (see Supplemental Material [34]) that the linear expansion coefficient is well approximated by $\alpha \sim -\pi \rho_F^2/4$. Therefore, the spin-excitation spectrum within this approximation is given by a simple expression involving only the DOS at E_F and the Stoner parameter:

$$\operatorname{Im}\chi(\omega) = \frac{\pi}{4} \frac{\rho_F^2 \omega}{(1 - I_s \rho_F)^2 + (\frac{\pi}{4} I_s \rho_F^2 \omega)^2}.$$
 (2)

By extracting ρ_F and I_s from our *ab initio* calculations, we have computed and displayed the expression predicted by Eq. (2) for each of the adatoms considered in Fig. 2 (see dashed lines). A comparison to the full *ab initio* calculations (solid lines) reveals a very good agreement for frequencies below 100 meV in the case of Rh, Ir, and Sc, where both the peak and width are properly described within $\leq 10\%$ relative error. This error is considerably larger in the case of Ni, indicating the importance of higher order expansion terms in ω for this case. Finally, the peak for Pd is far beyond the limit of small frequencies and therefore the approximation of Eq. (2) breaks down.

Proving Eq. (2) to be an accurate approximation of the full spin-excitation density given by Eq. (1) is extremely

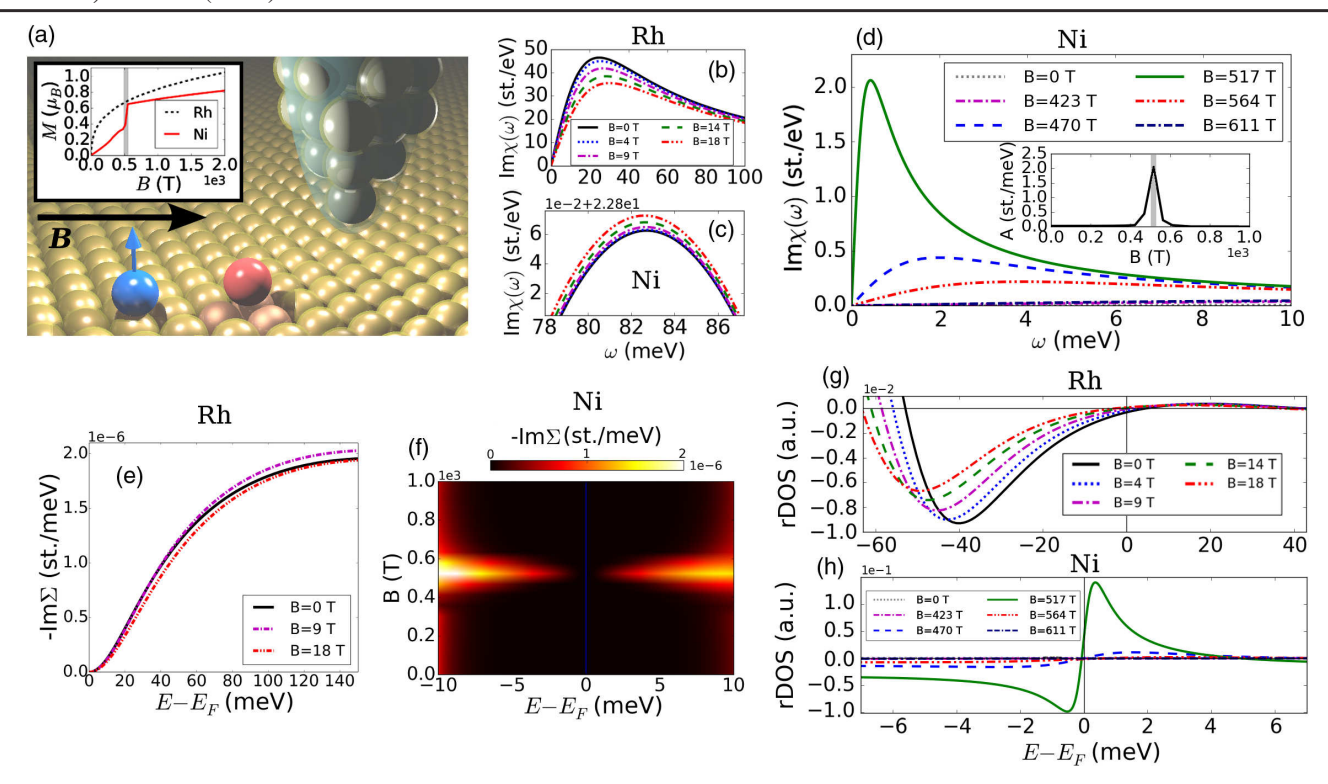


FIG. 3. (a) Minimal setup illustrating the proposed ISTS measurement. Substrate, nonmagnetic adatom, and tip atoms are displayed as gold, red, and grey balls, respectively, while the black arrow depicts an external magnetic field B. The graph in the inset illustrates the calculated magnetic moment M as a function of the external field for Rh and Ni adatoms, with the grey area indicating the critical regime of Ni where M shows a discontinuity. A blue ball with an arrow has been added in the main figure to illustrate the possibility of coupling a magnetic adatom to the nonmagnetic one, inducing on the later a magnetic moment of the order of the values shown in the inset, thus mimicking the effect of large magnetic fields [42]. The rest of the subfigures show the calculated magnetic field dependence of various properties. (b),(c) Density of PSE as given by $\text{Im}\chi(\omega)$ for Rh and Ni adatoms, respectively, for magnetic fields of up to 18 T (both figures share the same legend). (d) Same as in (c) but for larger magnetic fields of up to 10^3 T. The inset depicts the evolution of the PSE's amplitude [see Eq. (3)] as a function of the magnetic field. (e),(f) Imaginary part of the self-energy, $\text{Im}\Sigma(V_F)$, for Rh and Ni adatoms, respectively. Note the different scale of the magnetic field and the energy window in the two cases. Vertical (blue) line in (f) separates negative and positive energies. (g),(h) Energy derivative of the renormalized DOS (s orbital) for Rh and Ni, respectively. Note the difference in magnitude on the applied magnetic fields in both cases.

convenient, as the former provides an analytical interpretation for the origin of PSE in terms of just ρ_F and I_s , two basic electronic properties of adatoms. Indeed, the resonance frequency, linewidth, and amplitude of PSE predicted by Eq. (2) can be cast into simple expressions:

$$\omega_{\text{res}} = \frac{4}{\pi} \frac{|1 - I_s \rho_F|}{I_s \rho_F^2}, \qquad \Delta = 2\sqrt{3}\omega_{\text{res}},$$

$$A \equiv \text{Im}\chi(\omega_{\text{res}}) = \frac{1}{2I_s |1 - I_s \rho_F|}.$$
(3)

Interestingly, a potential measurement of the above quantities would directly yield experimental estimates for ρ_F and I_s . Upon closer inspection, one recognizes the Stoner product $I_s\rho_F$ as the key quantity in Eq. (3); as $I_s\rho_F \to 1$ (i.e., ferromagnetic instability), the resonance frequency as well as the linewidth tend to zero while the intensity of PSE shows a singularity. This analysis offers therefore the interpretation we sought for, namely, that elements closer

to the ferromagnetic instability show enhanced PSE, as it can be clearly checked from the comparison of Figs. 1 and 2. We emphasize that the mechanism just described is fundamentally different from the one taking place in magnetic adatoms, where the resonance frequency of transverse spin excitations is settled by the spin-orbit interaction via the magnetic anisotropy energy [40].

Having exposed the origin of PSE in single adatoms, we focus next on assessing their potential impact on the dI/dV signal as measured in ISTS experiments, the technique of choice for measuring magnetic excitations (see, e.g., Refs. [6,7,41]). The corresponding minimal setup is illustrated in Fig. 3(a), which displays a scanning tunneling microscope (STM) tip measuring the adatom's excitations under an applied external magnetic field, denoted as B. We first notice that PSE respond to magnetic fields by shifting their resonance frequency. This is quantitatively demonstrated in Figs. 3(b) and 3(c), where the calculated spinexcitation spectra are shown for Rh and Ni adatoms,

respectively, under B fields of ~10 T that are achievable in state-of-the-art laboratories (see, e.g., Refs. [7,24,25]). Noteworthily, while the PSE of Rh shifts towards larger frequencies as B is increased [see Fig. 3(b)], the PSE of Ni exhibits the opposite behavior [see Fig. 3(c)]. This difference arises from the fact that magnetic fields induce an effective modification of Stoner product, i.e., $I_s\rho_F \rightarrow \xi(B)I_s\rho_F$, where $\xi(B)$ is a term that depends both on the magnetic field as well as on the adatom's electronic structure (see Supplemental Material [34]). In particular, the details of the later make $\xi(B) > 1$ for Ni while $\xi(B) < 1$ for Rh, leading to the aforementioned divergent responses in accordance with Eq. (3).

Remarkably, when strong enough magnetic fields are applied to Ni, the modified Stoner criterion can be tuned towards the critical point, as shown in Fig. 3(d). As a consequence, the PSE's resonance frequency approaches the origin in a singular way while the amplitude of the excitation is enhanced by as much as 2 orders of magnitude for $B \sim 500$ T. It is interesting to note that this critical behavior is also present on the B-field dependence of the induced magnetic moment M, as shown in the inset of Fig. 3(a). While Rh shows a continuous dependence, Ni reveals a discontinuous transition at approximately the critical field value $B \sim 500$ T, above which the system enters a magnetic regime where the internal exchange field effectively contributes to M on top of the external Zeeman field, featuring the atomic version of a quantum phase transition. We note that, although such large B fields are clearly out of reach for current experiments, this feature could be potentially observed, e.g., via the proximity effect, by placing a magnetic adatom in the neighborhood of the nonmagnetic one [see Fig. 3(a)]. Our calculations verify that the former can induce on the later a magnetic moment of the same order of magnitude as the one induced by the fields of Fig. 3(d) [42], thus mimicking the action of large magnetic fields.

Next we evaluate the impact of PSE on the dI/dV signal of an ISTS measurement. For such purpose we consider the so-called Tersoff-Hamann approximation [43,44], which relates the ISTS spectrum to the electronic DOS at the tip position renormalized by the adatom's excitations. We access the latter quantity by means of a recently developed technique that combines many-body perturbation theory with our TDDFT scheme; details can be found in Ref. [45]. The central object within this formalism is the electron self-energy, Σ , which contains the interactions between the tunneling electrons from the tip at bias voltage V and the adatom's PSE. It is particularly revealing to inspect its imaginary part [45],

$$\operatorname{Im}\Sigma(V_F) = -I_s^2 \int_0^{-V} d\omega \rho(V_F + \omega) \operatorname{Im}\chi^*(\omega), \quad (4)$$

with $\rho(E)$ the energy-dependent DOS, $V_F = E_F + V$, and E_F the Fermi energy. The calculated Im $\Sigma(V_F)$ is shown in

Fig. 3(e) for Rh under various magnetic fields of up to 18 T. Our results reveal a clear step for positive bias voltage that saturates at ~100 meV, i.e., after the PSE peak has been integrated [see Eq. (4)]. Note also that the calculated self-energy slightly varies as a function of the magnetic field. When larger magnetic fields are applied, as illustrated in Fig. 3(f) for the case of Ni, the critical behavior of the PSE [see Fig. 3(d)] translates into a clear maximum at the value of the critical field, where ${\rm Im}\Sigma(V_F)$ increases by an order of magnitude.

The presence of PSE has a broad effect on the renormalization of the DOS at the vacuum, where ISTS tips measure the signal. In particular, the energy derivative of the renormalized DOS (rDOS) is a quantity that is linked to the d^2I/dV^2 curve measured by ISTS [45]. The former quantity is displayed in Fig. 3(g) for Rh, where the magnetic field dependence is clearly visible. Noteworthily, our calculations demonstrate that the tunneling electrons from the tip are able to trigger the PSE, leading to a peak in the meV region that, furthermore, reacts to external magnetic fields by shifting its resonance frequency as well as substantially modifying its intensity. We also note the strong asymmetric distribution between positive and negative frequencies, a feature that emerges from the background electronic structure [45] and is commonly present in d^2I/dV^2 curves measured on magnetic adatoms (see, e.g., Refs. [6,7, 46–48]). On the other hand, when Ni is driven into the critical regime as in Fig. 3(h), our calculations reveal a huge change of the signal's intensity as the PSE approaches the critical point. Our analysis therefore shows that magnetism offers a prime way of manipulating PSE, enabling us to discern them from other excitations of similar energy but nonmagnetic origin, such as phonons.

In conclusion, we have proposed and argued a means of detecting spin excitations in nonmagnetic single adatoms. We have shown that such excitations can develop welldefined peaks in the meV region, their main characteristics being determined by two fundamental electronic properties, namely, the Stoner parameter and the DOS at the Fermi level. Our analysis based on TDDFT has further revealed a pronounced dependence of PSE on externally applied magnetic fields, exhibiting the atomic analog of a quantum phase transition as the field approaches the critical value. This remarkable feature is likely to have strong effects in processes where a substantial magnetic moment is induced in nonmagnetic adatoms, e.g., when magnetic atoms are coupled to them via the proximity effect. Finally, we have simulated ab initio the impact of PSE on the d^2I/dV^2 curve measured in state-of-the-art ISTS experiments, revealing that PSE can be triggered by tunneling electrons and, furthermore, exhibit a clear response to magnetic fields. Thus, besides opening up potential applications for nonmagnetic adatoms, our analysis offers a route for experimentally accessing their fundamental electronic properties, such as the Stoner parameter.

This work has been supported by the Helmholtz Gemeinschaft Deutscher-Young Investigators Group Program No. VH-NG-717 (Functional Nanoscale Structure and Probe Simulation Laboratory), the Impuls und Vernetzungsfonds der Helmholtz-Gemeinschaft Postdoc Programme, and funding from the European Research Council (ERC) under the European Union's Horizon 2020 research and innovation program (ERC-consolidator Grant No. 681405 DYNASORE)

Note added in the proof.—In the recent work of Ref. [49], the conductance associated to a single Pd adatom deposited on Pd(111) has been experimentally measured and interpreted as being strongly affected by paramagnon scattering.

- *j.azpiroz@fz-juelich.de †s.lounis@fz-juelich.de
- [1] C. F. Hirjibehedin, C.-Y. Lin, A. F. Otte, M. Ternes, C. P. Lutz, B. A. Jones, and A. J. Heinrich, Science 317, 1199 (2007).
- [2] J. Fernández-Rossier, Phys. Rev. Lett. 102, 256802 (2009).
- [3] N. Lorente and J.-P. Gauyacq, Phys. Rev. Lett. 103, 176601 (2009).
- [4] S. Lounis, A. T. Costa, R. B. Muniz, and D. L. Mills, Phys. Rev. Lett. 105, 187205 (2010).
- [5] L. Zhou, J. Wiebe, S. Lounis, E. Vedmedenko, F. Meier, S. Blügel, P. H. Dederichs, and R. Wiesendanger, Nat. Phys. 6, 187 (2010).
- [6] A. A. Khajetoorians, S. Lounis, B. Chilian, A. T. Costa, L. Zhou, D. L. Mills, J. Wiebe, and R. Wiesendanger, Phys. Rev. Lett. 106, 037205 (2011).
- [7] A. A. Khajetoorians, T. Schlenk, B. Schweflinghaus, M. dos Santos Dias, M. Steinbrecher, M. Bouhassoune, S. Lounis, J. Wiebe, and R. Wiesendanger, Phys. Rev. Lett. 111, 157204 (2013).
- [8] M. Ternes, New J. Phys. 17, 063016 (2015).
- [9] A. A. Khajetoorians, M. Steinbrecher, M. Ternes, M. Bouhassoune, M. d. S. Dias, S. Lounis, J. Wiebe, and R. Wiesendanger, Nat. Commun. 7, 10620 (2016).
- [10] J. Ibañez-Azpiroz, M. dos Santos Dias, S. Blügel, and S. Lounis, Nano Lett. 16, 4305 (2016).
- [11] J. C. Oberg, M. R. Calvo, F. Delgado, M. Moro-Lagares, D. Serrate, D. Jacob, J. Fernández-Rossier, and C. F. Hirjibehedin, Nat. Nanotechnol. 9, 64 (2014).
- [12] S. Yan, D.-J. Choi, B. Jacob A. J., S. Rolf-Pissarczyk, and S. Loth, Nat. Nanotechnol. 10, 40 (2015).
- [13] A. Stróżecka, A. Eiguren, and J. I. Pascual, Phys. Rev. Lett. 107, 186805 (2011).
- [14] B. Bryant, R. Toskovic, A. Ferrn, J. L. Lado, A. Spinelli, J. Fernández-Rossier, and A. F. Otte, Nano Lett. 15, 6542 (2015).
- [15] S. Baumann, W. Paul, T. Choi, C. P. Lutz, A. Ardavan, and A. J. Heinrich, Science 350, 417 (2015).
- [16] F. Delgado and J. Fernández-Rossier, Prog. Surf. Sci. 92, 40 (2017).
- [17] S. Nadj-Perge, I. K. Drozdov, J. Li, H. Chen, S. Jeon, J. Seo, A. H. MacDonald, B. A. Bernevig, and A. Yazdani, Science 346, 602 (2014).

- [18] B. Braunecker and P. Simon, Phys. Rev. Lett. **111**, 147202 (2013).
- [19] M. M. Vazifeh and M. Franz, Phys. Rev. Lett. **111**, 206802 (2013).
- [20] M. Ternes, A. J. Heinrich, and W.-D. Schneider, J. Phys. Condens. Matter 21, 053001 (2009).
- [21] K. von Bergmann, M. Ternes, S. Loth, C. P. Lutz, and A. J. Heinrich, Phys. Rev. Lett. **114**, 076601 (2015).
- [22] P. Gambardella, S. Rusponi, M. Veronese, S. S. Dhesi, C. Grazioli, A. Dallmeyer, I. Cabria, R. Zeller, P. H. Dederichs, K. Kern *et al.*, Science 300, 1130 (2003).
- [23] B. Bryant, A. Spinelli, J. J. T. Wagenaar, M. Gerrits, and A. F. Otte, Phys. Rev. Lett. 111, 127203 (2013).
- [24] I. G. Rau, S. Baumann, S. Rusponi, F. Donati, S. Stepanow, L. Gragnaniello, J. Dreiser, C. Piamonteze, F. Nolting, S. Gangopadhyay *et al.*, Science 344, 988 (2014).
- [25] F. Donati, S. Rusponi, S. Stepanow, C. Wckerlin, A. Singha, L. Persichetti, R. Baltic, K. Diller, F. Patthey, E. Fernandes et al., Science 352, 318 (2016).
- [26] S. Doniach, Proc. Phys. Soc. London 91, 86 (1967).
- [27] R. Doubble, S. M. Hayden, P. Dai, H. A. Mook, J. R. Thompson, and C. D. Frost, Phys. Rev. Lett. 105, 027207 (2010).
- [28] J. B. Staunton, J. Poulter, B. Ginatempo, E. Bruno, and D. D. Johnson, Phys. Rev. B 62, 1075 (2000).
- [29] G. G. Lonzarich and L. Taillefer, J. Phys. C 18, 4339 (1985).
- [30] A. Aguayo, I. I. Mazin, and D. J. Singh, Phys. Rev. Lett. 92, 147201 (2004).
- [31] S. H. Vosko, L. Wilk, and M. Nusair, Can. J. Phys. 58, 1200 (1980).
- [32] N. Papanikolaou, R. Zeller, and P. H. Dederichs, J. Physics Cond. Matter 14, 2799 (2002).
- [33] S. Lounis, A. T. Costa, R. B. Muniz, and D. L. Mills, Phys. Rev. B 83, 035109 (2011).
- [34] See Supplemental Material at http://link.aps.org/supplemental/10.1103/PhysRevLett.119.017203, which includes Refs. [35–39], for computational details regarding DFT and TDDFT calculations, additional electronic properties of adatoms on Ag(100) and MgO/Ag(100), technical details on the calculation of the longitudinal KS spinsusceptibility and its frequency expansion.
- [35] P. Giannozzi, S. Baroni, N. Bonini, M. Calandra, R. Car, C. Cavazzoni, Davide Ceresoli, G. L. Chiarotti, M. Cococcioni, I. Dabo *et al.*, J. Phys. Cond. Matter **21**, 395502 (2009).
- [36] J. F. Janak, Phys. Rev. B 16, 255 (1977).
- [37] B. Lazarovits, L. Szunyogh, and P. Weinberger, Phys. Rev. B 65, 104441 (2002).
- [38] H. Beckmann and G. Bergmann, Phys. Rev. B 55, 14350 (1997).
- [39] K. Wildberger, P. Lang, R. Zeller, and P. H. Dederichs, Phys. Rev. B 52, 11502 (1995).
- [40] M. dos Santos Dias, B. Schweflinghaus, S. Blügel, and S. Lounis, Phys. Rev. B **91**, 075405 (2015).
- [41] M. Steinbrecher, A. Sonntag, M. d. S. Dias, M. Bouhassoune, S. Lounis, J. Wiebe, R. Wiesendanger, and A. A. Khajetoorians, Nat. Commun. 7, 10454 (2016).
- [42] For externally applied $B = 517 \,\mathrm{T}$ the magnetic moment of Ni is $m = 0.29 \,\mu_B$, while a Fe adatom placed as a second

- nearest neighbor induces a magnetic moment on Ni of $m = 0.51 \,\mu_B$.
- [43] J. Tersoff and D. R. Hamann, Phys. Rev. Lett. 50, 1998 (1983).
- [44] D. Wortmann, S. Heinze, P. Kurz, G. Bihlmayer, and S. Blügel, Phys. Rev. Lett. **86**, 4132 (2001).
- [45] B. Schweflinghaus, M. dos Santos Dias, A. T. Costa, and S. Lounis, Phys. Rev. B 89, 235439 (2014).
- [46] A. J. Heinrich, J. A. Gupta, C. P. Lutz, and D. M. Eigler, Science **306**, 466 (2004).
- [47] S. Holzberger, T. Schuh, S. Blügel, S. Lounis, and W. Wulfhekel, Phys. Rev. Lett. 110, 157206 (2013).
- [48] S. Baumann, F. Donati, S. Stepanow, S. Rusponi, W. Paul, S. Gangopadhyay, I. G. Rau, G. E. Pacchioni, L. Gragnaniello, M. Pivetta *et al.*, Phys. Rev. Lett. 115, 237202 (2015).
- [49] V. Schendel, C. Barreteau, M. Brandbyge, B. Borca, I. Pentegov, U. Schlickum, M. Ternes, P. Wahl, and K. Kern, arXiv:1702.02407.